# Experimental and Finite Element Studies of a 250kW Brushless Doubly Fed Induction Generator

Salman Abdi [1*], Ehsan Abdi [2], Richard McMahon [3]

[1] Faculty of Engineering, Environment and Computing, Coventry University, Priory Street, Coventry, UK
[2] Wind Technologies Limited, St John's Innovation Centre, Cambridge, UK
[3] Warwick Manufacturing Group (WMG), Warwick University, Coventry, UK
[*]Ac7019@coventry.ac.uk

**Abstract: This paper studies, using experimentally verified Finite Element analysis, various performance measures of the Brushless Doubly Fed Induction Generator (BDFIG) when magnetic wedges are used for closing stator open slots. The BDFIG is an attractive generator solution for offshore wind power and can replace doubly-fed slip-ring induction generators. It is shown in this paper that the use of magnetic wedges, commonly used in large induction machines, reduces the stator windings magnetising currents in a BDFIG, reflected in the values of magnetising inductances. They also increase the leakage flux in the stator slots, leading to a larger series inductance in the equivalent circuit. The series inductance significantly affects the BDFIG performance as well as the rating of its converter. The effects of magnetic wedges on BDFIG air gap flux, synchronous torque and stator tooth top saturation is also investigated. 2-D finite element analysis of an experimental 250 kW BDFIG is used in the study, verified by experimental measurements.**

## 1. Introduction

The Brushless Doubly-Fed Induction Generator (BDFIG) also known as Brushless Doubly Fed Machine (BDFM) is a variable speed generator or motor, which has in recent years been investigated as a potential replacement for the Doubly-Fed Induction Generator (DFIG) [1], currently used in the majority of large wind turbines. Similar to the DFIG concept, a BDFIG allows variable speed operation using only a fractionally-rated (30-50%) variable voltage, variable frequency converter [1]. The BDFIG has no brush gear and slip-rings, and hence is a robust and reliable machine with low maintenance requirements [2].

The BDFIG works in the synchronous mode when one of its stator windings, called the power winding (PW) is connected directly to the grid and the second stator winding, called the control winding (CW) is connected to a variable voltage variable frequency converter [1]. The synchronous mode is the desirable mode of operation for which the machine design and performance are optimised [3]. The pole numbers for stator windings are selected in a way to eliminate any direct coupling between the stator windings [4]. Instead, the coupling is enabled through a specially-designed rotor winding [5].

To date, several large BDFIGs have been manufactured, for instance a 75 kW machine in Brazil [6], a 200 kW size in China [7], and 250 kW machine in the UK, the largest size reported to date [8]. The latter was built and characterised by the authors and various aspects of its performance were reported in [8] and [9]. The 250 kW BDFIG was built in a frame size D400.

The 250 kW BDFIG was designed to include magnetic wedges in the stator slots to reduce the magnetising currents [10]. As in all induction machines, a larger air gap improves manufacturability but increases magnetising currents. Using magnetic wedges to close slot openings can reduce the effective air gap length resulting in lower magnetising currents and an improved power factor [11]. However, it will also increase the stator leakage inductance by providing a low reluctance path for leakage fluxes. The impact of magnetic wedges on the performance of induction and permanent magnet machines have been studied [11-12], but the effect of wedges is harder to predict in the BDFIG due to its complex design and magnetic field distribution [13]. The air gap contains two main fields with different pole numbers, normally at different angular velocities. Therefore, the motion of the flux is not a simple rotation, as in induction machines [14].

In this paper, the effects of magnetic wedges on the magnetic field patterns in the iron circuit of the BDFIG, air gap field and machine torque are studied using nonlinear finite element (FE) models. The accuracy of the FE model was verified by experimental measurements including stator currents and, using search coils, stator tooth and back iron fluxes.

The equivalent circuit is a convenient way of describing the steady-state performance of the machine [15]. The authors showed in [10] that stator magnetic wedges have a considerable effect on inductance values in the BDFIG equivalent circuit and proposed analytical methods to derive the stator magnetising and leakage inductances. Nevertheless, it is hard to obtain accurate estimates of certain parameters such as the slot leakage reactance from analytical methods. A more accurate method, which is explored in this paper, is to use the FE model to estimate the BDFIG equivalent circuit parameters. A curve fitting method was used to obtain the parameters from steady state performance data predicted by the FE model. The effects of magnetic wedges on BDFIG air gap flux, synchronous torque and stator tooth top saturation is also investigated using nonlinear FE models.

## 2. BDFIG Equivalent Circuit Model

A simplified equivalent circuit for the BDFIG is shown in Fig. 1 where all parameters are referred to the PW side and iron losses are neglected [15-16]. The circuit is valid for all modes of operation, including the induction, cascade and synchronous modes and can be utilized for the analysis of steady-state performance of the BDFIG [3]. The variables $s_1$ and $s_2$ are the power and control winding slips and are defined as:

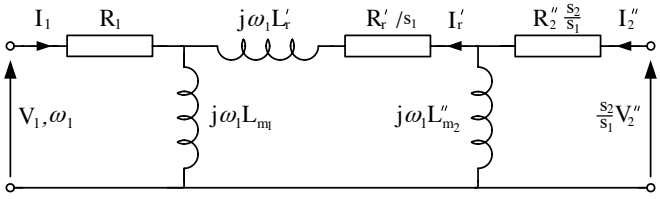


***Fig. 1.*** *Simplified equivalent circuit model for the BDFIG [14]*

$$s_1 = \frac{\omega_1 - p_1\omega_r}{\omega_1} \quad (1)$$

$$s_2 = \frac{\omega_2 - p_2\omega_r}{\omega_2} \quad (2)$$

where $\omega_1$ and $\omega_2$ are the angular frequencies of the PW and CW, and $\omega_r$ is the shaft angular speed. $p_1$ and $p_2$ are the PW and CW pole pair numbers, respectively.

The stator winding resistances, $R_1$ and $R_2$ may be calculated from the machine geometry at a certain operating temperature or preferably obtained from DC measurements. The magnetising inductances $L_{m1}$ and $L_{m2}$ are determined from the magnetising tests where a single stator winding is supplied in turn while the other winding is left open and the rotor is driven at the appropriate synchronous speed to eliminate rotor currents [15]. $L_r$ represents the series inductances in the full equivalent circuit, including the stator PW and CW and rotor leakage inductances [15]. It can be calculated from the machine geometry during the design stage using the method described in [4], it may also be estimated from applying a curve fitting method to the steady-state performance data including torque and currents obtained from the BDFIG in cascade operation [15]. The steady-state data may be provided from numerical models or experimental tests.

## 3. Finite Element Model

### *3.1. Prototype Machine Specifications*

Table 1 gives details of the prototype 250 kW BDFIG used in this study. Both the stator PW and CW are connected in delta. The rotor is a nested-loop design comprising six nests, each with five loops. All rotor loops are terminated with a common end-ring at one end only [8]. The machine is shown in Fig. 2 on the experimental rig. The machine's control cabinet including grid-side inverter (GSI) and machine-side inverter (MSI) is shown in Fig. 3. The GSI was developed with an embedded control system to stabilise the DC-link and synchronise to the 690 V grid voltage. The MSI was developed to control the PW real and reactive power using a Speedgoat controller.

### *3.2. BDFIG Finite Element Modelling*

The finite element analysis of the 250 kW BDFIG was performed using a commercial software application EFFE [17]. The model was solved as a voltage-fed problem so that simulation results can be compared directly to experimental measurements. A 2-D FE analysis was performed to reduce the computational time by assuming that the effects of axial flux are negligible. The end region leakage effects were incorporated into the analysis using lumped parameters. The modelling was performed using the time-stepping method for accurate analysis and took into account the nonlinear properties of the iron circuit.

**Table 1** 250 kW BDFIG specification

| | |
|---|---|
| Frame size | D400 |
| PW pole-pair number | 2 |
| PW rated voltage | 690V at 50Hz (delta) |
| PW rated current | 178 A (line) |
| CW pole-pair number | 4 |
| CW rated voltage | 620V at 18Hz (delta) |
| CW rated current | 74 A (line) |
| Speed range | 500 rpm ± 33% |
| Rated torque | 3700 Nm |
| Rated power | 250 kW |
| Efficiency | > 96% |
| Stack length | 820 mm |

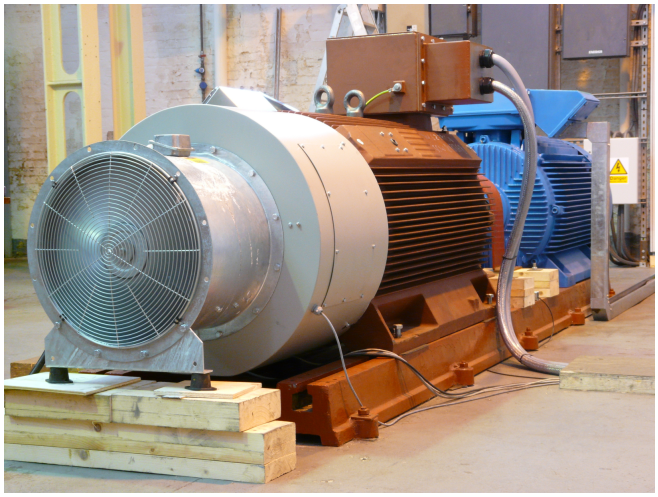

***Fig. 2.*** *250 kW BDFIG and the load machine on test rig.*

In the synchronous mode of operation, the PW is connected directly to the grid and the CW is supplied with variable voltage at variable frequency from a converter. The implementation of BDFIG synchronous operation in FE is particularly challenging because the CW excitation voltage required to set a specific load condition cannot be predetermined as the machine is not stable in open-loop.

Therefore, a closed-loop controller was implemented with details described in [18].

Two FE models were developed for the BDFIG, one with magnetic wedges present in the stator slot openings (FE-SYNC-W) as in the experimental BDFIG, and one with slots left open (FE-SYNC-NW). The magnetic properties of magnetic wedges and stator and rotor laminations were given by the machine manufacturer.

***Fig. 3.*** *250 kW BDFIG grid-side inverter (GSI) on the left-hand side, and machine-side inverter (MSI) on the right-hand side.*

In order to verify the accuracy of the FE model, the operating conditions as used in of an experimental test conducted in the synchronous mode were used, as shown in Table 2. The BDFIG was run at 650 rpm under rated voltages and torque. The stator PW and CW currents predicted by FE-SYNC-W are compared with the measurements in Fig. 4 and the rms values of currents are given in Table 3, showing that the FE results are in close agreement with the experimental data. Fig. 5 shows the magnetic flux distribution in the machine iron circuit obtained from the FE-SYNC-W model. Due to the 180º symmetry in BDFIG's flux pattern, only half of the machine cross section is analysed to reduce models' computational time.

**Table 2** Experimental operating conditions in the synchronous mode

| | | | |
|---|---|---|---|
| Speed (rev/min) | 650 | $f_{4-pole}$ (Hz) | 50 |
| Torque (Nm) | 3600 | $\lvert V_{8-pole}\rvert$ (V) | 610 |
| $\lvert V_{4-pole}\rvert$ (V) | 690 | $f_{8-pole}$ (Hz) | 15 |

Search coils were fitted into the BDFIG to measure the flux densities in a stator tooth and the back iron, as shown in Fig. 6 [19]. The measured magnetic fields under the operating conditions of Table 2 are compared with FE predictions in Fig. 7. The close agreement validates the use of FE modelling in the analysis of stator tooth flux presented in Section 5.

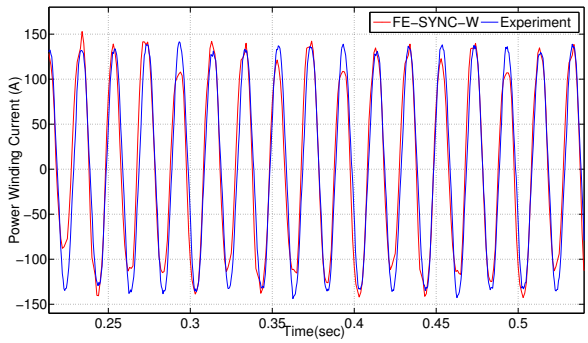


*(a) Stator PW current*

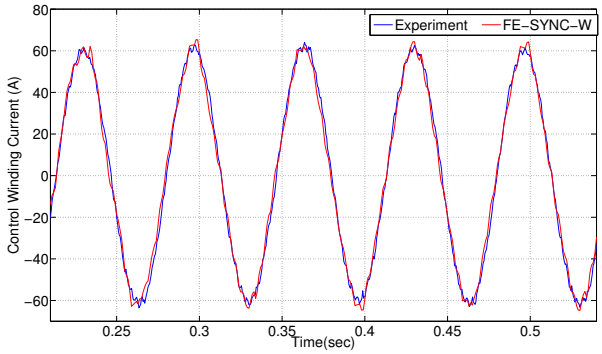


*(b) Stator CW current*

***Fig. 4.*** *Comparison of stator currents obtained from experimental tests and nonlinear FE model.*

**Table 3** Stator winding currents obtained from nonlinear FE model and experimental measurements.

| | $I_{PW}$ (A) | $I_{CW}$ (A) |
|---|---|---|
| FE-SYNC-W | 96.6 | 42.1 |
| Measurement | 97.1 | 43.3 |
| Difference | 0.5% | 2.8% |

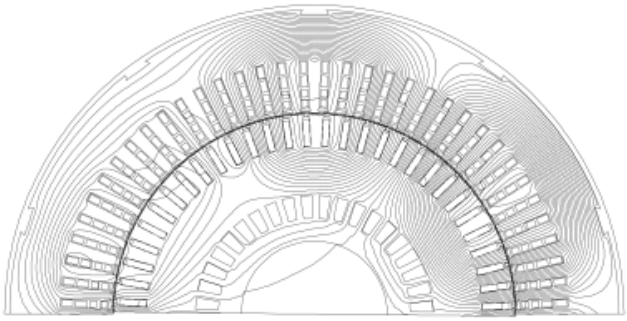

***Fig. 5.*** *BDFIG magnetic field distribution in the synchronous mode of operation (see Table 2) obtained from nonlinear FE simulation.*

### *3.3. Effect of Magnetic Wedges on BDFIG Magnetisation*

Fig. 8 compares the magnetic field pattern linking stator and rotor iron circuits for the two FE-SYNC-W and FE-SYNC-NW models, again with the machine operating at the conditions given in Table 2. It is evident that the field lines linking the stator and rotor find a low reluctance path

through the magnetic wedges than when the slots are left open. In the absence of magnetic wedges, the linking magnetic fields travel longer distance in air, leading to higher magnetising currents and hence larger magnetising inductances.

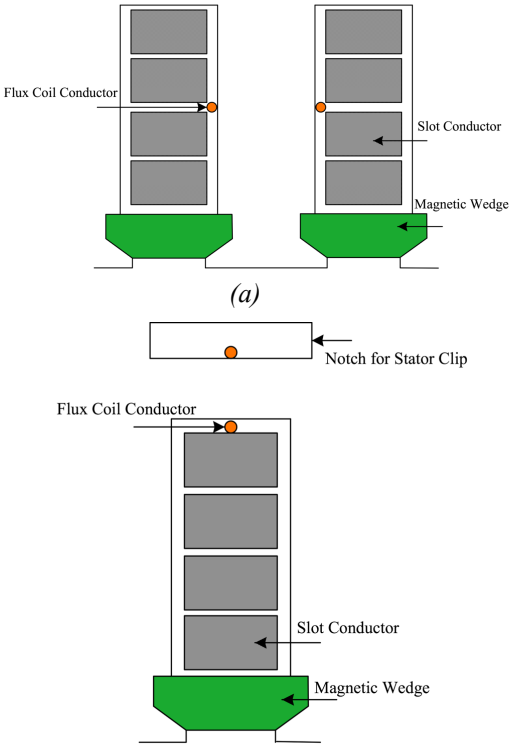


***Fig. 6.*** *Stator flux search coils fitted on to (a) stator tooth (b) stator back iron*

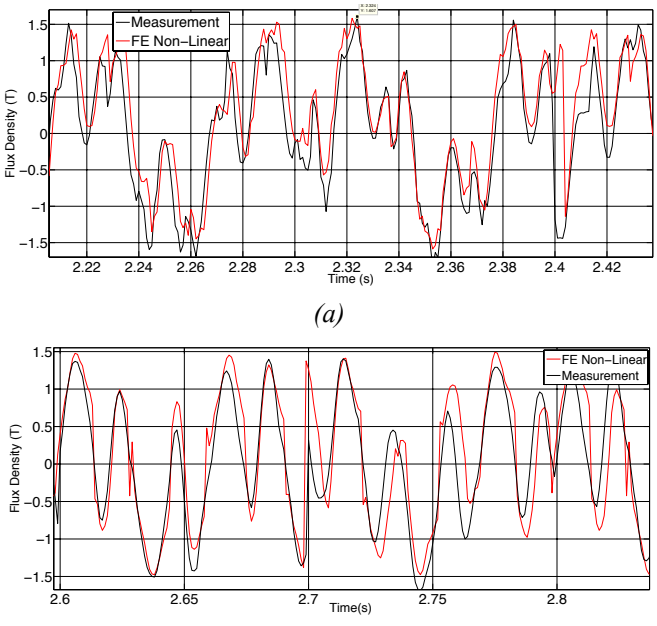


***Fig. 7.*** *Measured and predicted flux density in (a) stator tooth (b) stator back iron*

### *3.4. Effect of Magnetic Wedges on Stator Slot Leakage*

The low reluctance path for the magnetic fields through the magnetic wedges leads to an increased leakage flux, as shown in Fig. 9. Thus, the leakage inductances of the stator PW and CW increase as a result of using the magnetic wedge, reflected in a larger series inductance *Lr*.

## 4. Equivalent Circuit Parameter Estimation

The magnetising inductance in an electrical machine's equivalent circuit corresponds to the magnetic flux that links the stator and rotor, passing the air gap twice. The effects of stator and rotor slotting in the magnetising inductance are often modelled by Carter factors, which effectively scale the air gap length [20]. The effect of magnetic wedges in reducing magnetising currents, hence increasing magnetising inductances, can also be modelled by scaling the air gap length, similar to the concept of Carter factors. A modified Carter factor was proposed for the BDFIG by the authors in [10], which takes into account the effect of both slotting and magnetic wedges.

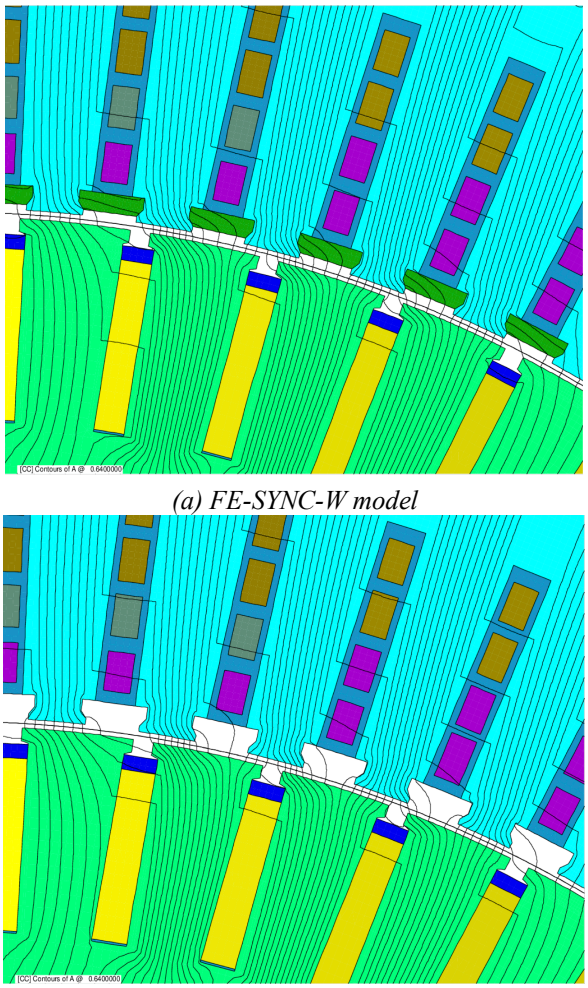

*(a) FE-SYNC-W model*

*(b) FE-SYNC-NW model*

***Fig. 8.*** *Magnetic flux lines linking stator and rotor magnetic circuits obtained from nonlinear FE models in the synchronous mode of operation: (a) FE-SYNC-W includes stator magnetic wedges, and (b) FE-SYNC-NW includes open slots.*

The equivalent circuit parameters can be estimated from steady-state performance data obtained from experimental tests or FE modelling. The magnetising inductances can be derived from magnetising tests

conducted in the induction mode [15]. The series inductance $L_r$ and rotor resistance $R_r$ can then be estimated using curve fitting methods applied to the results from cascade tests [15]. Table 4 shows the values of stator windings magnetising inductances, $L_{m1}$ and $L_{m2}$, and the referred series inductance $L'_r$ obtained from FE-SYNC-NW and FE-SYNC-W models and experimental tests. As can be seen, there is close agreement between the parameter values obtained from the FE-SYNC-W model (which resembles the experimental BDFIG with magnetic wedges fitted) and experiments, confirming that the FE method is a suitable tool for determining the equivalent circuit parameters.

In addition, it can be seen from Table 4 that the inductance values obtained for a machine with open slots i.e. FE-SYNC-NW are considerably lower than those of the machine with magnetic wedges i.e. FE-SYNC-W and experiments. This validates the findings in Section 3 that the magnetic wedges provide a low reluctance path for magnetic fields, making the linkage between stator and rotor achieved through smaller magnetising currents (i.e. larger magnetising inductances), but at the same time, bridging between adjacent teeth and thus increasing the leakage flux (i.e. larger series inductance).

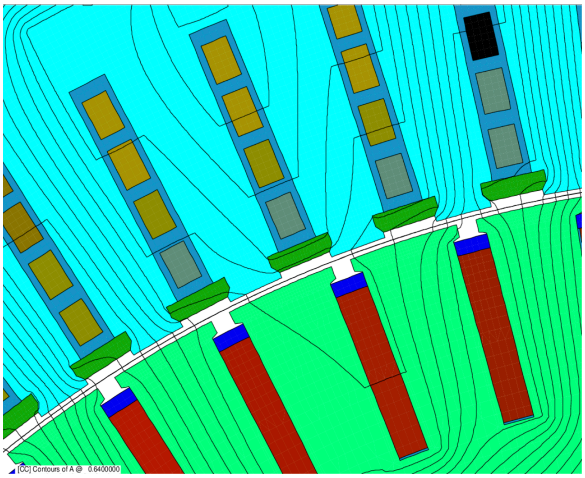

*(a) FE-SYNC-W model*

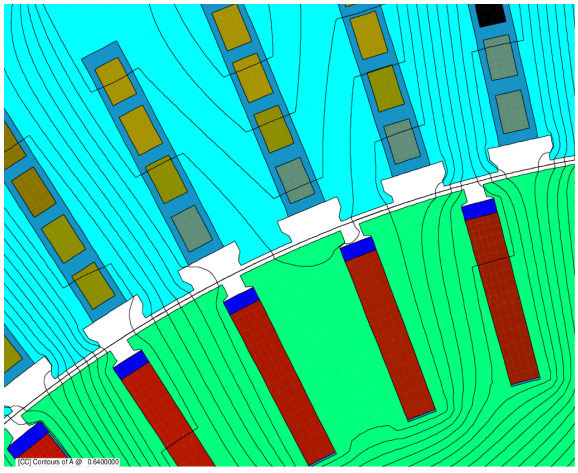

*(b) FE-SYNC-NW model*

***Fig. 9.*** *Comparison of slot leakage flux (a) with stator magnetic wedges and (b) open slots. The magnetic wedge in the middle slot in figure (a) bridges the magnetic field between two adjacent teeth, resulting in a higher leakage flux.*

**Table 4** BDFIG equivalent circuit parameter values

| | | $L_{m1}$ (mH) | $L_{m2}$ (mH) | $L'_r$ (mH) |
|---|---|---|---|---|
| No magnetic wedge | FE-SYNC-NW | 84 | 284 | 9.7 |
| With magnetic wedge | FE-SYNC-W | 97 | 341 | 13.3 |
| | Experiment | 104 | 368 | 12.5 |

## 5. Stator Tooth Flux Density

Fig. 10 shows the magnetic flux density distribution in the top region of a stator tooth, obtained from FE-SYNC-NW and FE-SYNC-W models under the operating conditions of Table 2. Various locations are numbered from 1 to 8 and the peak flux densities at those locations are compared between the two models, i.e. with and without stator magnetic wedges, in Table 5. As shown, the peak flux densities are closely matched between the two models for locations 1 to 4.

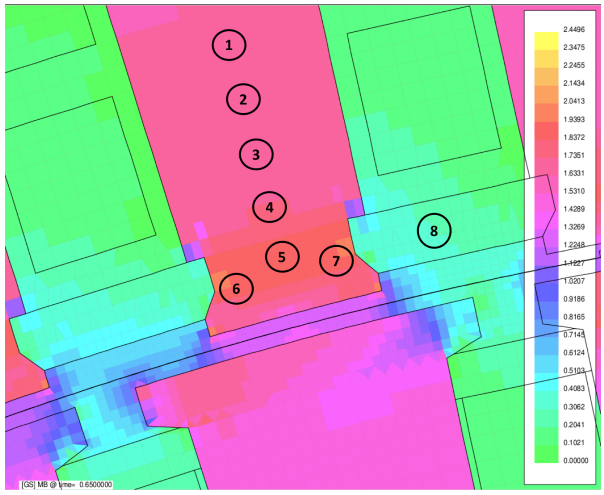


*(a)*

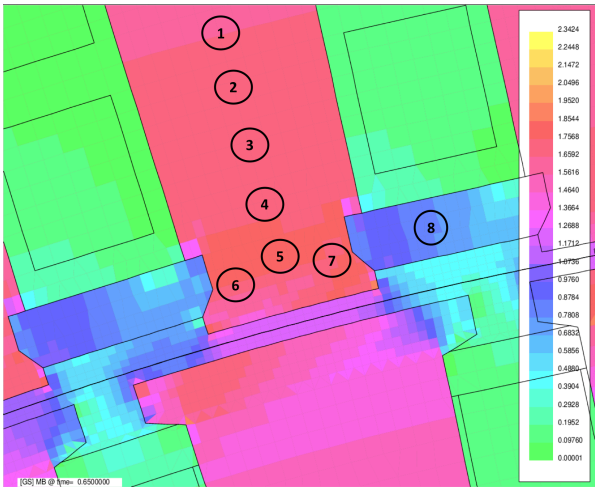


*(b)*

***Fig. 10.*** *Magnetic flux density distribution in the top region of stator tooth in (a) FE-SYNC-NW model and (b) FE-SYNC-W model.*

However, the difference between the peak flux densities in the stator tooth top, i.e. locations 5 to 7, is considerable. A degree of saturation is seen in the stator tooth top in the case of open slot design, where the peak flux densities reach 1.95 to 2.14 T.

On the other hand, when magnetic wedges are used, the peak flux density in the stator tooth top is lower than 1.88 T, avoiding undue saturation. This is mainly achieved through the contribution of magnetic wedges in accommodating part of the flux linkage between the stator and rotor, as evident from the peak flux density inside the magnetic wedge i.e. location 8.

**Table 5** Values of peak flux densities in different locations specified in Fig. 10.

| | B1 (T) | B2 (T) | B3 (T) | B4 (T) | B5 (T) | B6 (T) | B7 (T) | B8 (T) |
|---|---|---|---|---|---|---|---|---|
| FE-SYNC-NW | 1.68 | 1.70 | 1.73 | 1.83 | 1.95 | 2.05 | 2.14 | 0.23 |
| FE-SYNC-W | 1.65 | 1.66 | 1.69 | 1.77 | 1.83 | 1.88 | 1.87 | 0.84 |

## 6. BDFIG's Performance at Synchronous Mode of Operation

### *6.1. Air Gap Flux and Torque Harmonic Mitigation*

As shown in the previous section, the stator magnetic wedges contribute to the magnetic circuit, especially in the flux linkage between the stator and rotor. It is therefore expected that the air gap flux density to be smoother when magnetic wedges are used than the case with open slots. Fig. 11 shows the air gap flux density obtained from the two FE models FE-SYNC-NW and FE-SYNC-W and a Fast Fourier Transform (FFT) analysis of the two fluxes. As anticipated, there is significant reduction in the harmonic level of the air gap flux when magnetic wedges are used.

The more uniform air gap flux density results in a smoother torque. Fig. 12 compares the rated torque ripple predicted by the FE-SYNC-NW and FE-SYNC-W models at the same load conditions. The torque plot obtained from FE-SYNC-W has intentionally been shifted down in Fig. 12a to separate the torque plots and hence enable better comparison of the torque ripple. As expected, the machine with stator magnetic wedges has a smoother torque.

### *6.2. Power Factors and Efficiency*

As seen in Section 6.1, the magnetic wedges used for closing the stator slots caused reduction in the harmonic magnitudes of the air gap flux density in the BDFIG, known as tooth ripples [21]. This effect can result in lower stator pole surface losses and efficiency improvements [22]. In addition, as stated in Section 4, the magnetising inductance values of the stator PW and CW are increased in the presence of magnetic wedges leading to reduction in the required PW and CW magnetising currents and hence further improving the efficiency and machine's power factors. Table 6 compares the no-load currents and full-load efficiency and power factors of the prototype machine obtained from FE-SYNC-W and FE-SYNC-NW models. The input power of the BDFIG can be calculated as:

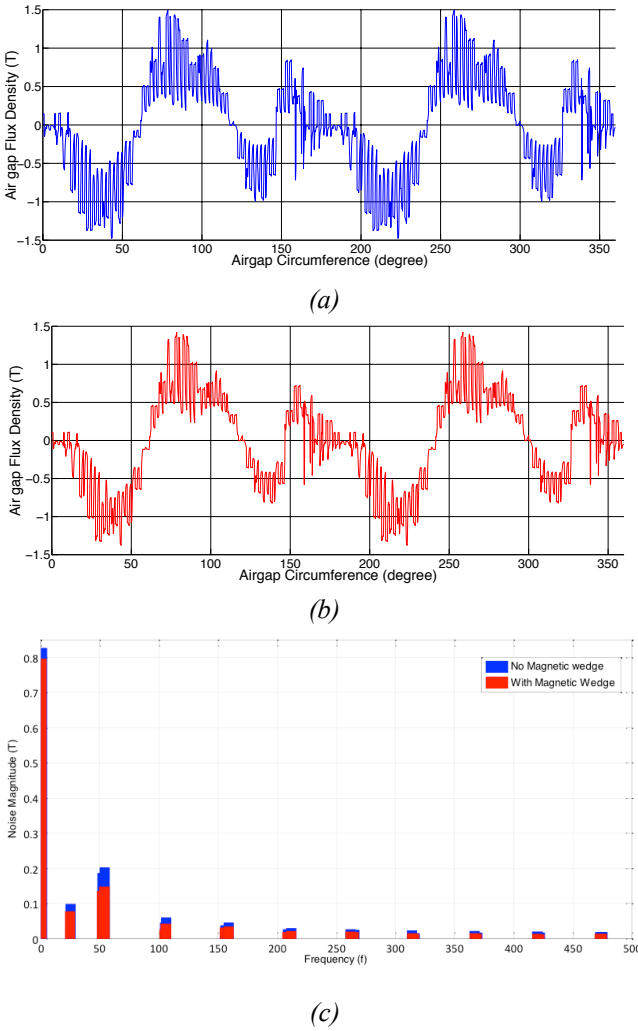


***Fig. 11.*** *Air gap flux density obtained from (a) FE-SYNC-NW and (b) FE-SYNC-W models; and (c) FFT analysis of air gap flux density.*

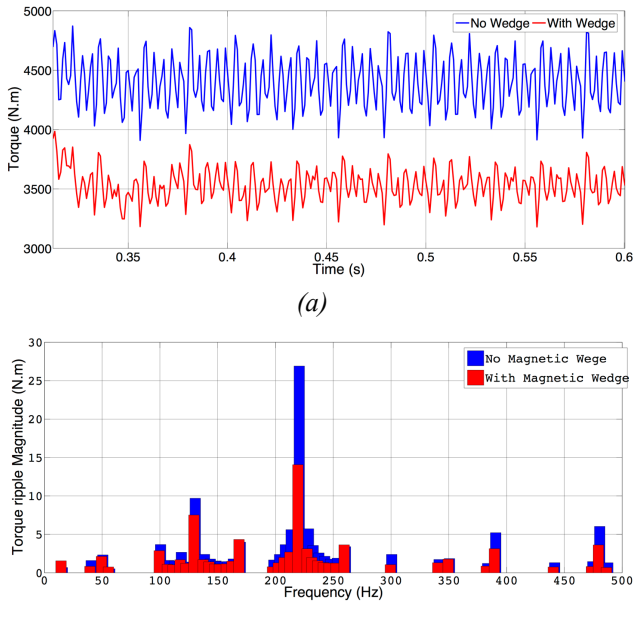


***Fig. 12.*** *(a) Synchronous torque obtained from FE-SYNC-NW and FE-SYNC-W models, and (b) FFT analysis of torque ripple.*

$$P_{in} = 3\left\{V_{PW}^{ph} I_{PW}^{ph} \cos\phi_{PW} + V_{CW}^{ph} I_{CW}^{ph} \cos\phi_{CW}\right\} \quad (3)$$

Where $V_{PW}^{ph}$ and $V_{CW}^{ph}$ are the PW and CW supplied phase voltages, $I_{PW}^{ph}$ and $I_{CW}^{ph}$ are the PW and CW phase currents, and $\cos\phi_{PW}$ and $\cos\phi_{PW}$ are the PW and CW power factors. The machine's output power can also be determined by taking an average of the rotor mechanical power at steady state operation:

$$P_{out} = \frac{1}{\Delta t}\int_{t_1}^{t_2} T_{out}\omega_r \, dt \quad (4)$$

As shown in Table 6, the power factors for both PW and CW were increased noticeably in the presence of magnetic wedges. This is expected based on the results obtained at no load conditions where both PW and CW no-load currents were decreased significantly in the presence of magnetic wedges. Furthermore, the machine's full-load efficiency was improved by 0.2% with magnetic wedges used for closing the stator slots. This is essentially due to smoother air gap flux density, which results in lower iron losses, as well as lower magnetizing currents leading to lower stator copper losses. It should be noted that the rotor mechanical losses were ignored for both FE-SYNC-W and FE-SYNC-NW models.

**Table 6** Efficiency and power factor comparison of FE-SYNC-NW and FE-SYNC-W models.

| | **FE-SYNC-NW** | **FE-SYNC-W** |
|---|---|---|
| Torque | 3583 Nm | 3581 Nm |
| PW No-Load Current | 26.71 A | 23.36 A |
| PW Power Factor | 0.87 | 0.89 |
| CW No-Load Current | 19.32 A | 16.27 A |
| CW Power Factor | 0.78 | 0.81 |
| Input Power | 241.2 kW | 239.8 kW |
| Output Power | 220.2 kW | 219.4 kW |
| Full-Load Efficiency | 91.3% | 91.5% |

## 7. Conclusion

This paper has shown that the use of stator magnetic wedges in the BDFIG can significantly increase the magnetising inductances whilst at the same time significantly increase the stator slot leakage and hence the series inductance in the equivalent circuit. The series inductance directly affects several operating aspects of the BDFIG, such as the converter rating, reactive power management and low-voltage ride-through performance. Therefore, the design and use of magnetic wedges should be carefully considered prior to the construction of a large-scale BDFIG.

It has also been shown that the use of magnetic wedges reduces undue saturation in the stator tooth top, the harmonics in the air gap flux and ripple in the machine's torque. This is mainly due to the contribution of magnetic wedges to the magnetic circuit of the BDFIG.

A finite element (FE) modelling has been used for the BDFIG and shown to give predictions close to experimental measurements. The FE is a powerful tool to check and optimise the BDFIG magnetic circuit, but also provides data in order to obtain estimated equivalent circuit parameters.

## 8. References


[1] McMahon, R., Wang, X., Abdi-Jalebi, E., Tavner, P., Roberts, P., Jagiela, M.: 'The BDFM as a generator in wind turbines.' 12th International Power Electronics and Motion Control Conference, EPE- PEMC, September 2006.

[2] Tavner, P., Higgins, A., Arabian, H., Long, T., Feng, Y.: 'Using an FMEA method to compare prospective wind turbine design reliabilities'. European Wind Energy Conf. 2010 Technical Track, Warsaw, Poland, April 2010.

[3] Tohidi, S.: 'Analysis and simplified modelling of brushless doubly-fed induction machine in synchronous mode of operation', IET Electric Power Applications, Vol. 10, Issue 2, 2016.

[4] Roberts, P., Long, T., McMahon, R., Shao, S., Abdi, E.: 'Dynamic modelling of the brushless doubly fed machine', IET Electric Power Applications, Vol. 7, Issue 7, 2013.

[5] McMahon, R., Tavner, P., Abdi, E., Malliband, P., Barker, D.: 'Characterising brushless doubly fed machine rotors', IET Electric Power Applications, vol. 7, pp. 535 – 543, 2013.

[6] Carlson, R., Voltolini, H., Runcos, F., Kuo-Peng, P., Baristela, N.: 'Performance analysis with power factor compensation of a 75 kw brushless doubly fed induction generator prototype.', IEEE International Conference on Electric Machines and Drives, 2010.

[7] Liu, H., Xu, L.: 'Design and performance analysis of a doubly excited brushless machine for wind power generator application.', IEEE International Symposium on Power Electronics for Distributed Generation Systems, 2010, pp. 597 – 601.

[8] Abdi, E., McMahon, R., Malliband, P., Shao, S., Mathekga, M., Tavner, P., Abdi, S., Oraee, A., Long, T., Tatlow, M.: 'Performance analysis and testing of a 250 kw medium-speed brushless doubly fed induction generator', Renewable Power Generation, IET, vol. 7, no. 6, pp. 631 – 638, 2013.

[9] Long, T., Shao, S., Malliband, P., Abdi, E., McMahon, R.: 'Crowbarless Fault Ride-Through of the Brushless Doubly Fed Induction Generator in a Wind Turbine Under Symmetrical Voltage Dips', IEEE Transactions on Industrial Electronics, Vol. 60, Issue 7, 2013.

[10] Abdi, S., Abdi, E., Oraee, A., McMahon, R.: 'Equivalent Circuit Parameters for Large Brushless Doubly

Fed Machines (BDFMs)', IEEE Trans. Energy Conversion, vol. 29, no. 3, pp. 706 – 715, 2014.

[11] Donato, G., Capponi, F., and Caricchi, F.: 'No-load performance of axial flux permanent magnet machines mounting magnetic wedges', IEEE Transactions on Industrial Electronics, vol. 59, no. 10, pp. 3768 – 3779, 2012.

[12] Kappatou, J., Gyftakis, K., Safacas, A.: 'A study of the effects of the stator slot wedges material on the behaviour of an induction machine', Portugal: International Conference on Electrical Machines, 2008.

[13] Abdi, E., Malliband, P., McMahon, R.: 'Study of iron saturation in brushless doubly-fed induction machines', Atlanta: Energy Conversion Congress and Exposition (ECCE), November 2010, pp. 3501 – 3508

[14] Abdi, S., Abdi, E., Oraee, A., McMahon, R.: 'Optimization of Magnetic Circuit for Brushless Doubly Fed Machines', IEEE Trans. Energy Conversion, vol. 30, no. 4, pp. 1611 – 1620, 2015.

[15] Roberts, P., McMahon, R., Tavner, P., Maciejowski, J., Flack, T.: 'Equivalent circuit for the brushless doubly fed machine (BDFM) including parameter estimation and experimental verification', IEE Proceedings - Electric Power Applications, Vol. 152, Issue 4, 2005, pp. 933-942.

[16] McMahon, R., Roberts, P., Wang, X., Tavner, P.: 'Performance of BDFM as generator and motor', Electrical Power Applications, IEE Proceedings, vol. 153, no. 2, pp. 289–299, March 2006.

[17] Abdi, S., Abdi, E., McMahon, M.: 'A Study of Unbalanced Magnetic Pull in Brushless Doubly Fed Machines', IEEE Trans. Energy Conversion, DOI: 10.1109/TEC.2015.2394912, 2015.

[18] Mathekga, M., Shao, S., Logan, T., McMahon, R.: "Implementation of a pi phase angle controller for finite element analysis of the BDFM." Bristol: Power Electronics, Machines and Drives (PEMD), 6th IET International Conference on, March 2012, pp. 1–6.

[19] Abdi, E.: 'Modelling and instrumentation of brushless doubly-fed (induction) machines', Ph.D. dissertation, University of Cambridge, Cambridge, U.K., 2006.

[20] Carter, F.: 'Note on air gap and interpolar induction', J. Inst. Electr. Eng., vol. 29, pp. 925–933, 1900.

[21] Madescu, G., Greconici, M., Biriescu, M., Mot, M.: 'Effects of Stator Slot Magnetic Wedges on the Induction Motor Performances', International conference on optimization of electrical and electronic equipment (OPTIM), May 2012, pp. 489 – 492.

[22] Takeda, Y., Yagisawa, T., Suyama, A., Yamamoto, M., 'Application of Magnetic Wedges to Large Motors', IEEE Transactions on Magnetics, Vol. 20, No 5, September 1984.